

Validity of the Generalized Density Matrix Method for Microscopic Calculation of Collective/Bosonic Hamiltonian

L. Y. Jia^{1,*} and V. G. Zelevinsky¹

¹*National Superconducting Cyclotron Laboratory and Department of Physics and Astronomy, Michigan State University, East Lansing, Michigan 48824, USA*

(Dated: June 8, 2018)

Recently a procedure by generalized density matrix (GDM) is proposed [1] for calculating a collective/bosonic Hamiltonian microscopically from the shell-model Hamiltonian. In this work we examine the validity of the method by comparing the GDM results with that of the exact shell-model diagonalization in a number of models. It is shown that the GDM method reproduces the low-lying collective states quite well, both for energies and transition rates, across the whole region going from vibrational to γ -unstable and deformed nuclei.

PACS numbers: 21.60.Ev, 21.10.Re,
Keywords:

It is a long-standing problem in nuclear physics to understand how macroscopic collective motion arises from microscopic single-particle motion. The shell-model (configuration interaction) successfully reproduces various collective behaviors by diagonalizing the nucleon Hamiltonian in a huge Slater-determinant basis. However, the dimension of the basis makes it impractical except for the cases with only a few valence nucleons. On the other hand, phenomenological bosonic approaches are often successful in fitting the experimental data (first of all the geometric Bohr Hamiltonian [2, 3] and the interacting boson model [4]). This shows that, out of the huge Slater-determinant space, there exists a few degrees of freedom with a bosonic nature, which are usually enough in describing the collective states. Serious efforts were devoted to deriving those parameters of the bosonic Hamiltonian from the underlying shell-model Hamiltonian. However, the complete theory is still missing.

Recently we proposed [1] a procedure based on the generalized density matrix (GDM) that was originally formulated in Refs. [5–8]. This procedure is rather simple, clean, and consistent. In compact form, there are only two equations, (14) and (23) in Ref. [1]. Results from the lowest orders give the well-known Hatree-Fock (HF) equations and random phase approximation (RPA). Higher orders fix the anharmonic terms in the collective/bosonic Hamiltonian. The aim of this work is to demonstrate the validity of the GDM method, by comparing its results with that of the exact shell-model diagonalization.

In this work for simplicity we restrict ourselves to systems without rotational symmetry. The GDM formulation with angular-momentum vector coupling has been considered in Ref [9]. The single particle (s.p.) space in this work is drawn schematically in Fig. 1. There are two degenerate s.p. levels with energies $e = \pm 1/2$. The Fermi surface is in between, thus the lower levels are completely

filled and upper levels are empty. Each s.p. level has a quantum number m that is a half integer. Degenerate time-reversal pair has m with different sign, $m_{\bar{1}} = -m_1$. For fermions, $|\bar{1}\rangle = -|1\rangle$, and we choose the phases such that

$$|\tilde{m}\rangle = |-m\rangle \quad , \quad |-\tilde{m}\rangle = -|m\rangle \quad (m > 0).$$

We assume a two-body Hamiltonian,

$$H = \sum_{12} f_{12} a_1^\dagger a_2 + \frac{1}{4} \sum_{1234} V_{1234} N[a_1^\dagger a_2^\dagger a_3 a_4], \quad (1)$$

where $f_{12} = \delta_{12} e_1$, e_1 are the HF s.p. energies shown in Fig. 1. The density matrix $\rho_{12} = \delta_{12} n_1$, where the occupation number $n_1 = 1(0)$ for the lower(upper) s.p. levels. $N[a_1^\dagger a_2^\dagger a_3 a_4]$ is the normal-ordering form of operators. The residual interaction is of $Q \cdot Q$ type,

$$V_{1234} = -\kappa(q_{14}q_{23} - q_{13}q_{24}),$$

where the moment operator $Q = \sum_{12} q_{12} a_1^\dagger a_2$ is Hermitian and time-even. For simplicity we assume q is real, thus

$$q_{12} = q_{21} = q_{\bar{2}\bar{1}} = q_{\bar{1}\bar{2}}.$$

Operator q has certain selection rule with respect to quantum number m , which will be specified later. We further set diagonal matrix elements of q to zero, $q_{11} = 0$; hence the moment of the mean field vanishes, $Q^{(00)} = \text{Tr}[q\rho] = 0$.

Following the procedure in Ref. [1], we are able to map the fermionic Hamiltonian (1) onto a bosonic Hamiltonian

$$H_b = \omega^2 \frac{\alpha^2}{2} + \frac{\pi^2}{2} + \Lambda^{(30)} \frac{\alpha^3}{3!} + \Lambda^{(12)} \frac{\{\alpha, \pi^2\}}{4} + \Lambda^{(40)} \frac{\alpha^4}{4!} + \Lambda^{(22)} \frac{\{\alpha^2, \pi^2\}}{8} + \Lambda^{(04)} \frac{\pi^4}{4!} + \Lambda^{(50)} \frac{\alpha^5}{5!} + \dots, \quad (2)$$

where the collective coordinate α and momentum π satisfy $[\alpha, \pi] = i$. Meanwhile, the generalized density matrix

*Electronic address: jial@nscl.msu.edu

$r^{(mn)}$ in the expansion

$$R_{12} \equiv a_2^\dagger a_1 = \rho_{12} + r_{12}^{(10)} \alpha + r_{12}^{(01)} \pi + r_{12}^{(20)} \frac{\alpha^2}{2} + \dots \quad (3)$$

is expressed in terms of $\Lambda^{(mn)}$. The bosonic Hamiltonian H_b (2) should reproduce the low-lying collective spectrum of the original nucleon Hamiltonian H (1). Substituting the solution (3) into $Q = \sum_{12} q_{12} a_1^\dagger a_2$, we get the boson image of the latter,

$$Q_b = Q^{(10)} \alpha + Q^{(20)} \frac{\alpha^2}{2} + Q^{(02)} \frac{\pi^2}{2} + Q^{(30)} \frac{\alpha^3}{3!} + \dots, \quad (4)$$

where $Q^{(mn)} = \text{Tr}[qr^{(mn)}]$, and time-odd terms vanish automatically. The transition rates calculated from Q_b between eigenstates of H_b should reproduce that of Q between eigenstates of H .

As stated in Ref. [1], the GDM method fixes H_b completely. In each even order (quadratic, quartic ...) in H_b , the GDM method gives one constraint on $\Lambda^{(mn)}$'s. The number of constraints is the same as that of independent parameters in H_b , removing in Eq. (2) superficial degrees of freedom due to canonical transformations of α and π conserving $[\alpha, \pi] = i$.

In the following we consider four models with different structures (different configurations of s.p. levels and different selection rules of q). We start with the simplest case of the first model. Both the upper and lower group have 12 degenerate s.p. levels with quantum numbers $m = \pm\frac{1}{2}, \pm\frac{3}{2}, \dots, \pm\frac{11}{2}$. Operator q has the selection rule $\Delta m = 0$, that is, q_{12} vanishes unless $m_1 = m_2$. The non-vanishing q_{12} ($m_1 = m_2$) are set to be 1.

In this model we find by numerical computation a ‘‘symmetry’’. That is, there are only three non-vanishing terms in Hamiltonian (2): ω^2 , $\Lambda^{(40)}$, and $\Lambda^{(22)}$ (besides $\pi^2/2$). We suspect there was some kind of ‘‘quasi angular-momentum symmetry’’, similar to that in the Lipkin model, where the only three non-vanishing terms are ω^2 , $\Lambda^{(40)}$, and $\Lambda^{(04)}$ (see Ref. [1]).

The results are shown in Fig. 2. We see that the GDM calculation reproduces the exact results of the shell model quite well, both for energies and transition rates. In the shell model we calculate the lowest several states by Lanczos method. The dashed line in the upper panel is the beginning of the s.p. continuum, only those collective states below the continuum can be seen. In the GDM calculation the resultant bosonic Hamiltonian is diagonalized in a finite ‘‘physical’’ bosonic space, $\{|0 \leq n \leq 12\}$. $|n\rangle$ is the n phonon state, $A^\dagger A|n\rangle = n|n\rangle$, $A^\dagger = (u\alpha + iv\pi)/\sqrt{2}$, $uv = -1$. The coefficient u is fixed by minimizing $A|\text{HF}\rangle$ in its one-particle-one-hole components, where $|\text{HF}\rangle$ is the Hartree-Fock ground state that is mapped onto the bosonic state $|n = 0\rangle$. The result is $u^4 = \frac{\sum_{2 < F < 1} |r_{12}^{(10)}|^2}{\sum_{2 < F < 1} |r_{12}^{(01)}|^2}$, where the summation indices 1 and 2 run over unoccupied and occupied s.p. levels, respectively (‘‘F’’ means Fermi surface). In models of this

work, u is a number close to 1. The shown GDM energies and transitions are practically independent of small variations of u around the above value.

As κ increases, the system goes from vibrational to γ -unstable region. In the vibrational region, higher excited states are influenced more by the anharmonicities, as expected. At large κ the spectrum becomes doubly degenerate in a deep double-well potential (large negative ω^2).

We would like to mention an important point, that the GDM method works better with increasing Ω (collectivity). Another calculation has been done (but not shown here) with 8 particles in 16 s.p. levels. The GDM results of the current calculation (12 particles in 24 s.p. levels) have very clear improvement over that of the former. In other words, the error in Fig. 2 may be of order $1/\Omega$. The largest part of this error may come from the RPA frequency ω^2 . At the current stage, the GDM method calculates all $\Lambda^{(mn)}$ in their leading order of $1/\Omega$ but not the next. We suspect that the correct $\omega^2 = \Lambda^{(20)}$ is smaller by a $1/\Omega$ term than the one determined here by the RPA equation. This would shift all the GDM curves to the left (smaller κ) a little bit, which would decrease greatly the systematic error (see Fig. 2). This systematic error own to ω^2 seems to be present in all models in this work (see Figs. 3-5). Also, it is confirmed in the Lipkin model where everything is known analytically (see Ref. [1]). Hence an apparent improvement would be calculating ω^2 in its next-to-leading order of $1/\Omega$.

Next we consider the second model, which has the same s.p. configuration but a different q that now has the selection rule $\Delta m = 0, \pm 1$. Non-vanishing q_{12} is still set to be 1. In this model we did not find a ‘‘symmetry’’ as in the previous case, so the problem exists of what should be the ‘‘best’’ mapping. In the following we did three sets of GDM calculations. The first calculation keeps only $\Lambda^{(40)}$ (besides $\omega^2 \alpha^2/2$ and $\pi^2/2$) in H_b , which is fixed by the constraint from 4th order in e.o.m. The second calculation keeps only $\Lambda^{(40)}$ and $\Lambda^{(60)}$, which are fixed by the two constraints from upto 6th order in e.o.m. The third calculation keeps only $\Lambda^{(40)}$, $\Lambda^{(22)}$, and $\Lambda^{(04)}$, fixed by the three constraints from upto 8th order in e.o.m.

We first notice in Fig. 3 that in this model the s.p. continuum goes down as increasing κ , as opposed to going up in the previous model. This is because now mixing of s.p. levels within the upper(lower) group is allowed by the selection rule that Δm can be ± 1 . As a result, originally degenerate levels from the upper(lower) group get a finite spread, which decreases the gap of the s.p. continuum. Only the first excited state is below the gap and calculated in the shell model.

In the GDM calculations we see that the simplest one degree-of-freedom ($\Lambda^{(40)}$) calculation is reasonably well in most cases except at very large κ . The other two calculations ($\Lambda^{(40/60)}$ and $\Lambda^{(40/22/04)}$) give essentially the same results (for the quantities shown in Fig. 3), although their common parameter, $\Lambda^{(40)}$, differ a lot. This insensitivity of GDM results to the degrees of freedom

chosen, is important. As we said, two different bosonic Hamiltonians could be equivalent if they were related by canonical transformations/renormalizations of variables α and π . This insensitivity simply says that the GDM formalism knows these renormalizations and does them correctly. In the first model we also find this insensitivity (but not shown). Finally we notice that in regions of $\omega^2 \sim 1/\Omega$, calculations that go to higher orders in e.o.m. may give unphysical results. This is again because the e.o.m. are accurate in leading order of $1/\Omega$ but not the next. The fact that this “divergence” appears slightly before the instability point of RPA shown in Fig. 3, indicates again that the correct ω^2 may be smaller than the one calculated by RPA, as mentioned before.

At last we consider two models with s.p. configuration that is asymmetric in upper and lower groups, which generates odd anharmonicities that are necessary for deformation. In the third model, the lower group has 10 s.p. levels with $m = \pm\frac{3}{2}, \dots, \pm\frac{11}{2}$, the upper group has 14 s.p. levels with $m = \pm\frac{1}{2}, \dots, \pm\frac{13}{2}$. In the fourth model, the lower group has 12 s.p. levels with $m = \pm\frac{1}{2}, \dots, \pm\frac{11}{2}$, the upper group has 10 s.p. levels with $m = \pm\frac{1}{2}, \dots, \pm\frac{9}{2}$. In both models, operator q still has the selection rule of $\Delta m = 0, \pm 1$, with non-vanishing matrix elements set to be 1. The third model has a slightly larger asymmetry than that of the fourth model, and their signs of the asymmetry are different.

These two models are more complicated in the sense that now there are more active degrees of freedom (odd anharmonicities). In the GDM method, we do a possibly simplest calculation. We keep in H_b only $\Lambda^{(30)}$, $\Lambda^{(12)}$, and $\Lambda^{(40)}$ (besides $\omega^2\alpha^2/2$ and $\pi^2/2$). $\Lambda^{(30)}$ and $\Lambda^{(12)}$ are fixed by requiring $Q^{(20)} = Q^{(02)} = 0$ in the solution (4). Then $\Lambda^{(40)}$ is fixed by the constraint from 4th order in e.o.m. The requirement $Q^{(20)} = Q^{(02)} = 0$ is the same as that for previous two models without upper-lower asymmetry, by which $\Lambda^{(30)}$ and $\Lambda^{(12)}$ vanish.

The results are shown in Figs. 4-5. The deformation begins around the critical point of RPA when ω^2 becomes negative. In the vibrational region the potential is stiff and deformation is not easy. As κ increases, the potential becomes flat in bottom and finally of a double-well shape. Then, even a relatively small odd anharmonicity (here mainly $\Lambda^{(30)}$) can tilt the potential and generate large deformation. We notice firstly that the GDM calculations give the correct sign of deformations: positive/negative for the ground/first-excited state of the third model, and vice versa for the fourth model. In realistic situation $\Lambda^{(30)}((\hat{\alpha} \times \hat{\alpha})^2 \times \hat{\alpha})^0 \sim \Lambda^{(30)}\beta^3 \cos 3\gamma$ ($\hat{\alpha}$ is the quadrupole phonon and β, γ are Bohr angles), the sign of $\Lambda^{(30)}$ “determines” the intrinsic shape of the nucleus (prolate or oblate). This is especially interesting in the transitional regions where the rotor formula is not applicable. Secondly, the quantitative agreement of deformation is also good except at the largest κ .

There the deformation “saturates” towards its maximal possible value within the model space, favored by energy. Meanwhile in the boson mapping, we are too close to the boundary of the finite physical bosonic space, and the GDM results become inaccurate. In realistic nuclei this “saturation” may not be usual. The number of participating/active nucleons is usually around 30 in well-deformed nuclei, which is much larger than that around 10 in the current models. Finally, we would like to point out that the first excited state in our simple models is not a “rotational” state, rather it corresponds to the next “band head” in realistic rotational nuclei. The rotational states that are very low in energy come in only in three dimensions.

In this work we demonstrate the validity of the GDM procedure in microscopically calculating the collective/bosonic Hamiltonian. The lowest several states of this bosonic Hamiltonian quite well reproduce the collective states of the exact shell-model, both for energies and transition rates, in a wide range from vibrational, γ -unstable, to deformed nuclei. Specifically, we show that deformation can be described without introducing a deformed mean field. The traditional procedure of “symmetry breaking and restoration”, first “statically” breaks rotational symmetry in the ground state, by representing the latter as a Slater determinant of deformed s.p. levels (Nilsson levels); then projects afterwards to good angular momentum. However, in case of large shape fluctuations (flat minimal of energy surface) or shape coexistence (two close minimal), it may fail. On the other hand, the GDM procedure always conserves the rotational symmetry. Deformations are put in “dynamically” at higher orders (for example cubic terms) beyond the mean field. Thus it is suitable to describe for example shape fluctuation and coexistence problems.

In realistic nuclei, the gap of s.p. continuum is generated by the pairing correlations. The GDM formalism based on the Hartree-Fock-Bogoliubov transformation is straightforward and has been done in Ref. [9]. However, another treatment may be possible. Instead of introducing Bogoliubov quasi-particles and representing the ground state as a Slater determinant of the former, the pairing correlations are considered in higher orders beyond the mean field, by keeping both the particle-hole and particle-particle channels in the factorization $a_4^\dagger a_3^\dagger a_2 a_1 \approx a_4^\dagger a_1 \cdot a_3^\dagger a_2 - a_4^\dagger a_2 \cdot a_3^\dagger a_1 + a_4^\dagger a_3^\dagger \cdot a_2 a_1$. In this way the symmetry of exact particle number is always conserved. Work along this line is in progress and results seem promising. We are also generalizing the GDM code by including angular-momentum vector coupling that are necessary for realistic calculations.

This work is supported by the NSF grants PHY-0758099 and PHY-1068217.

-
- [1] L. Y. Jia, and V. G. Zelevinsky, Phys. Rev. C **84**, 064311 (2011).
 - [2] A. Bohr and B. Mottelson, *Nuclear Structure* (Benjamin, New York, 1975), Vol. 2.
 - [3] L. Prochniak and S. G. Rohozinski, J. Phys. G: Nucl. Part. Phys. **36**, 123101 (2009). /Topical review./
 - [4] A. Arima and F. Iachello, Ann. Rev. Nucl. Part. Sci. **31**, 75 (1981); F. Iachello and A. Arima, *the Interacting Boson Model* (Cambridge Univ. Press, 1987).
 - [5] A. Kerman and A. Klein, Phys. Rev. **132**, 1326 (1963).
 - [6] S.T. Belyaev and V.G. Zelevinsky, Yad. Fiz. **11**, 741 (1970) [Sov. J. Nucl. Phys. **11**, 416 (1970)]; Yad. Fiz. **16**, 1195 (1972) [Sov. J. Nucl. Phys. **16**, 657 (1973)]; Yad. Fiz. **17**, 525 (1973) [Sov. J. Nucl. Phys. **17**, 269 (1973)].
 - [7] V.G. Zelevinsky, Prog. Theor. Phys. Suppl. **74-75**, 251 (1983).
 - [8] M.I. Shtokman, Yad. Fiz. **22**, 479 (1975) [Sov. J. Nucl. Phys. **22**, 247 (1976)].
 - [9] L. Y. Jia, Phys. Rev. C **84**, 024318 (2011).

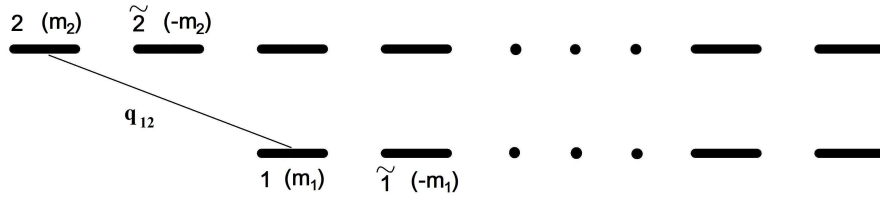


FIG. 1: Single-particle level scheme. $\tilde{1}$ is the time-reversal level of 1. Each level has a quantum number m .

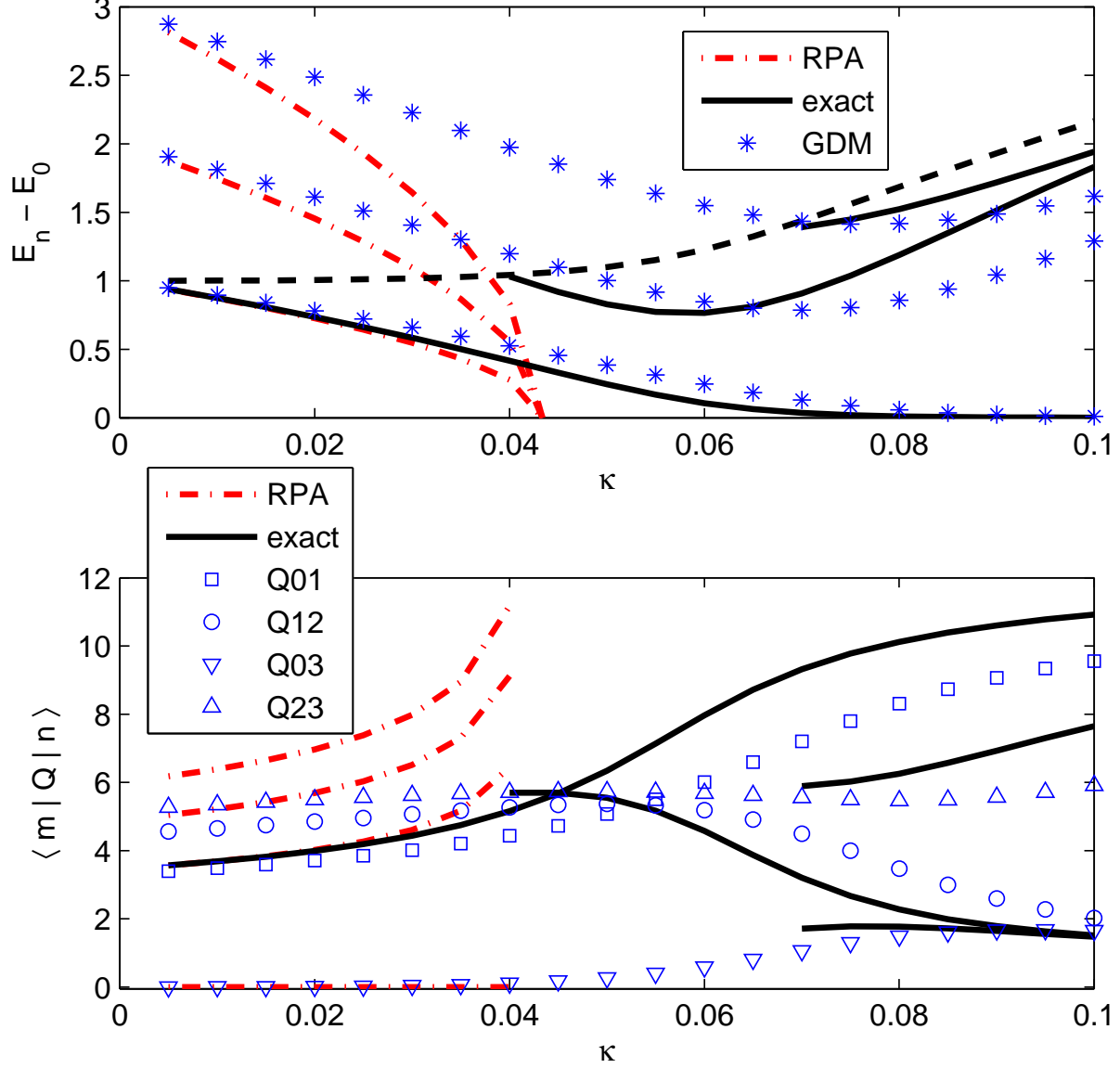


FIG. 2: (Color online) Excitation energies $E_n - E_0$ and transition matrix elements $\langle m|Q|n \rangle$ in the first model of this work as a function of κ . The black solid lines are exact results by shell-model diagonalization. The black dashed line is the beginning of the single particle continuum. The red dashed-dotted lines are the RPA results. The blue symbols are GDM results. The asterisks are energies; and the squares, circles, up-triangles and down-triangles are matrix elements of Q between different states. $\langle m|Q|n \rangle$ that are not shown vanish in both the shell model and the GDM calculations.

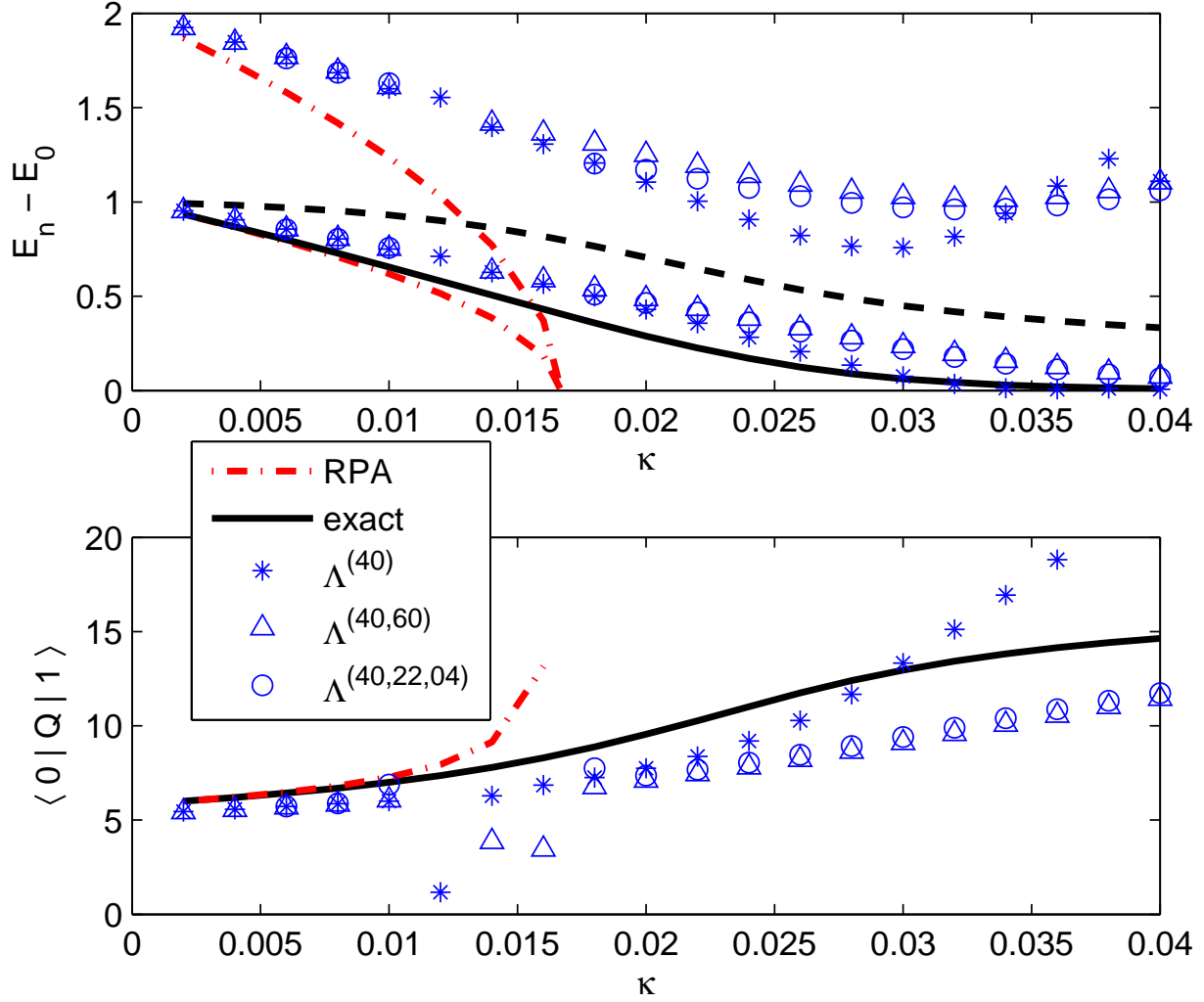


FIG. 3: (Color online) Excitation energies $E_n - E_0$ and transition matrix elements $\langle 0|Q|1 \rangle$ in the second model of this work as a function of κ . The black solid lines are exact results by shell-model diagonalization. The black dashed line is the beginning of the single particle continuum. The red dashed-dotted lines are the RPA results. The blue symbols (asterisks, up-triangles and circles) are results of three different sets of GDM calculations, as labeled in the legend.

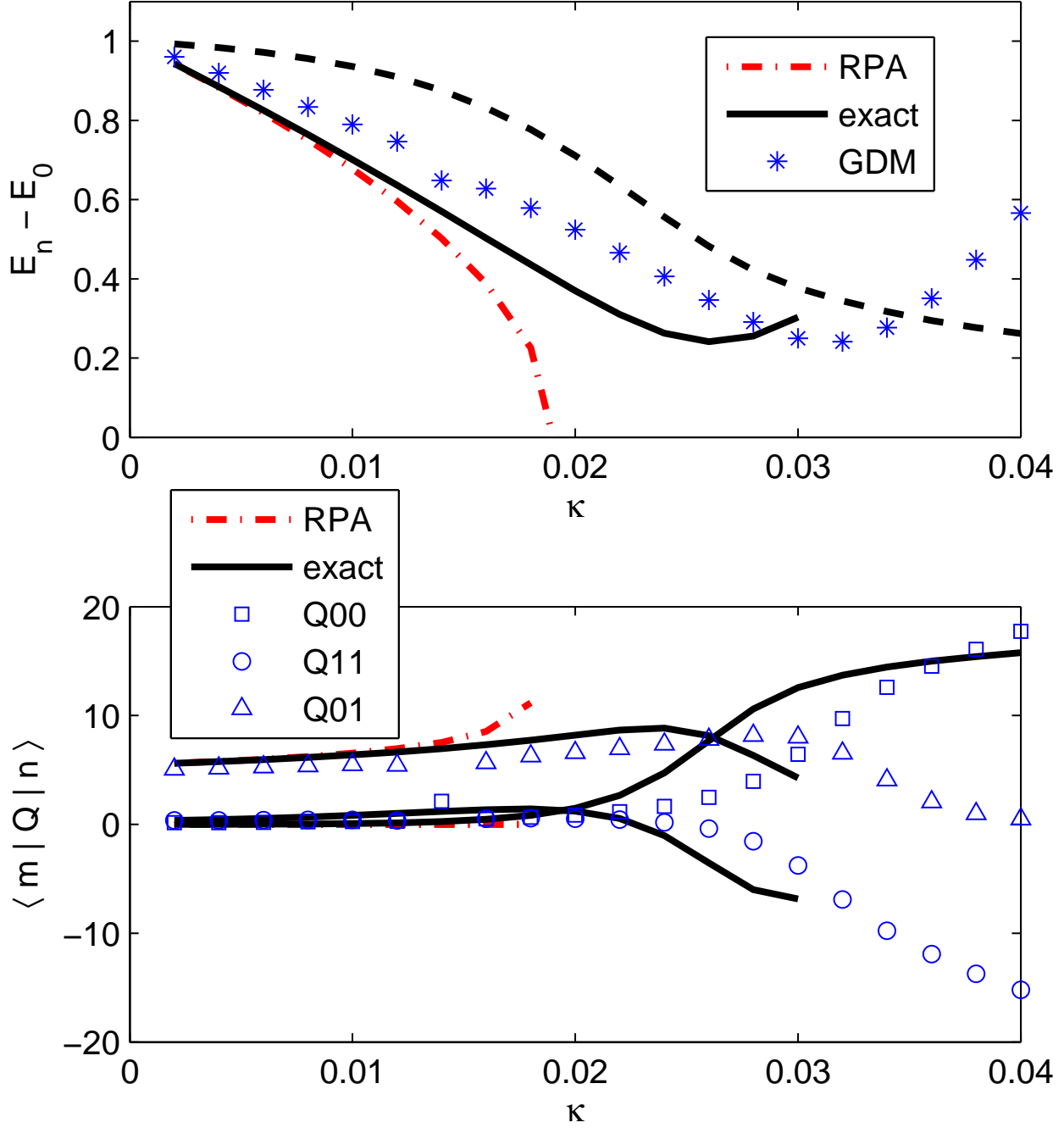


FIG. 4: (Color online) Excitation energies $E_n - E_0$ and transition matrix elements $\langle m|Q|n \rangle$ in the third model of this work as a function of κ . The black solid lines are exact results by shell-model diagonalization. The black dashed line is the beginning of the single particle continuum. The red dashed-dotted lines are the RPA results. The blue symbols are GDM results. The asterisks are energies; and the squares, circles and up-triangles are matrix elements of Q between different states.

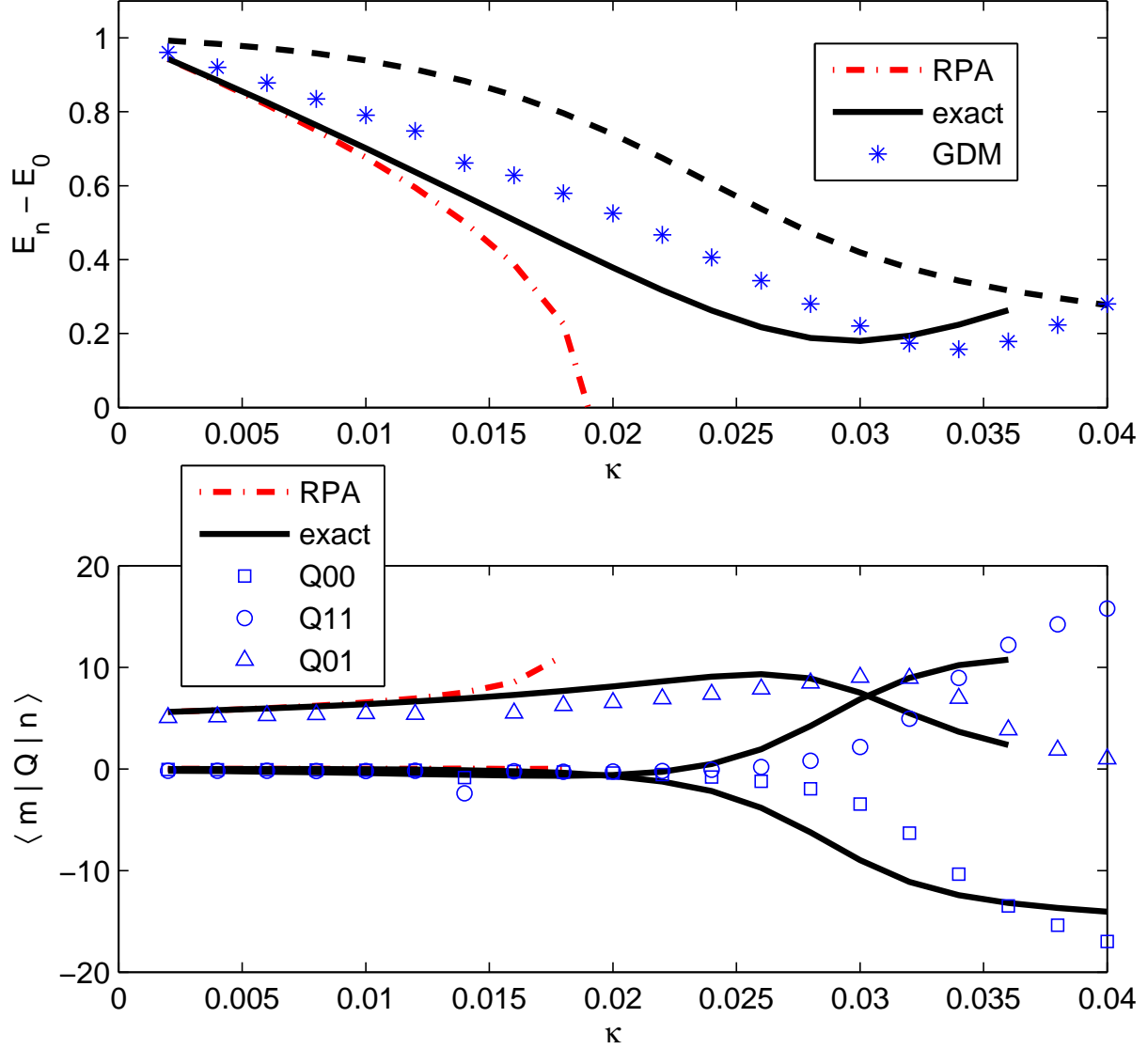


FIG. 5: (Color online) Excitation energies $E_n - E_0$ and transition matrix elements $\langle m|Q|n \rangle$ in the fourth model of this work as a function of κ . The black solid lines are exact results by shell-model diagonalization. The black dashed line is the beginning of the single particle continuum. The red dashed-dotted lines are the RPA results. The blue symbols are GDM results. The asterisks are energies; and the squares, circles and up-triangles are matrix elements of Q between different states.